Solid Freeform Fabrication 2023: Proceedings of the 34th Annual International Solid Freeform Fabrication Symposium – An Additive Manufacturing Conference
Reviewed Paper

Developing Additively Manufactured Iron Powder-filled PLA Composites

Jeevan Kumar*, Orkhan Huseynov*, Ismail Fidan[¥], and Mustafa Rajabali[#]

*Department of Mechanical Engineering, Tennessee Technological University, Cookeville, TN 38505
[¥]Department of Manufacturing and Engineering Technology, Tennessee Technological University, Cookeville, TN 38505
[#]Department of Physics, Tennessee Technological University, Cookeville, TN 38505

Abstract

The Low-Cost Metal Material Extrusion (LCMMEX) process has gained attention in recent years to produce metallic parts with complex designs. High Iron concentration composite materials have been extensively researched to improve their properties and functionality for advanced manufacturing applications. This study aims to develop knowledge blocks for producing composite parts with high iron percentages and analyze their physical properties based on print parameters. A rectangular sample is manufactured using the Material Extrusion (MEX) process, with variations in layer height, infill density, and print speed. The investigation shows that a number of parameters affects the change in surface roughness, weight, and dimensional accuracy of the printed parts. Furthermore, an increase in the infill percentage leads to a significant increase in magnetic flux. This research study provides insights into the influence of print parameters on the properties of high-iron-filled composite parts, ideal for high-density applications.

Introduction

Additive Manufacturing (AM) is a technology that enables the production of three-dimensional objects by adding material layer by layer. Its capabilities in creating complex geometries and customized parts with high accuracy and precision make it valuable across industries such as aerospace, automotive, medical, and consumer goods [1].

The American Society for Testing and Materials (ASTM) has standardized seven cores AM processes that utilize the layer-by-layer approach to shape desired geometries and produce final parts as per customer requirements. While the materials used may vary across these processes, the fundamental fabrication methods remain consistent. For a comprehensive understanding of the layer-by-layer AM process, Figure 1 offers a detailed visual representation with corresponding descriptions, serving as a helpful reference [2].

Among the seven common AM technologies, which are presented in Figure 2. MEX is widely applicable in various industries today [3]. It is a popular method for producing lightweight parts with customized shapes. Additionally, MEX is ideal for rapid prototyping and fulfilling diverse customer needs [4]. MEX employs various materials like Acrylonitrile butadiene styrene (ABS), Polylactic acid (PLA), nylon, glass-filled nylon, High Impact Polystyrene (HIPS), and Polyvinyl Alcohol (PVA) [5, 6]. The process involves a machine that extrudes filament from a spool through a nozzle, using a stepper motor to place the material layer by layer onto the build plate. The layer thickness is in the range of 0.07 mm to 0.8 mm depending

on the part built and its settings. The final part is built in the x, y, and z directions, and once printing is complete, the machine produces a finished product depending on the requirements [7].

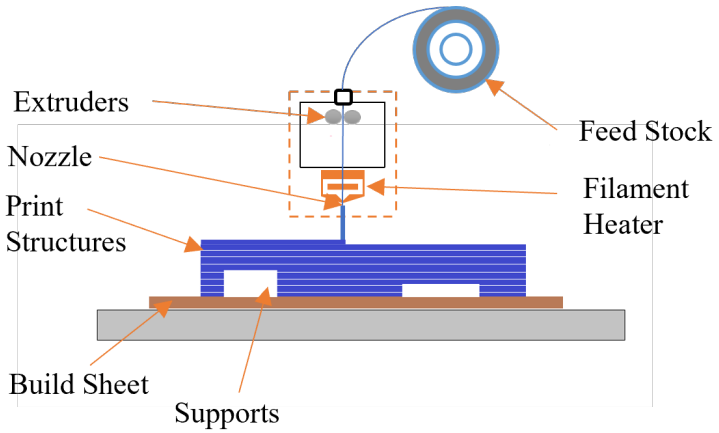

Figure 1 MEX Printer Layout

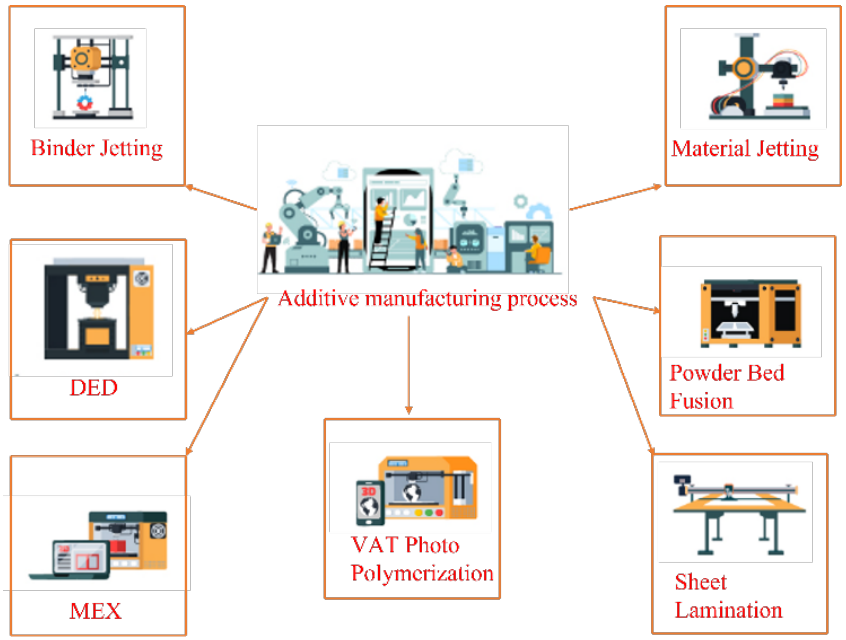

Figure 2 Seven Different Types of AM

AM has undergone significant advancements since its inception in the 1980s. Figure 3 depicts the timeline of AM technology, highlighting significant milestones and innovations in the field [8–10].

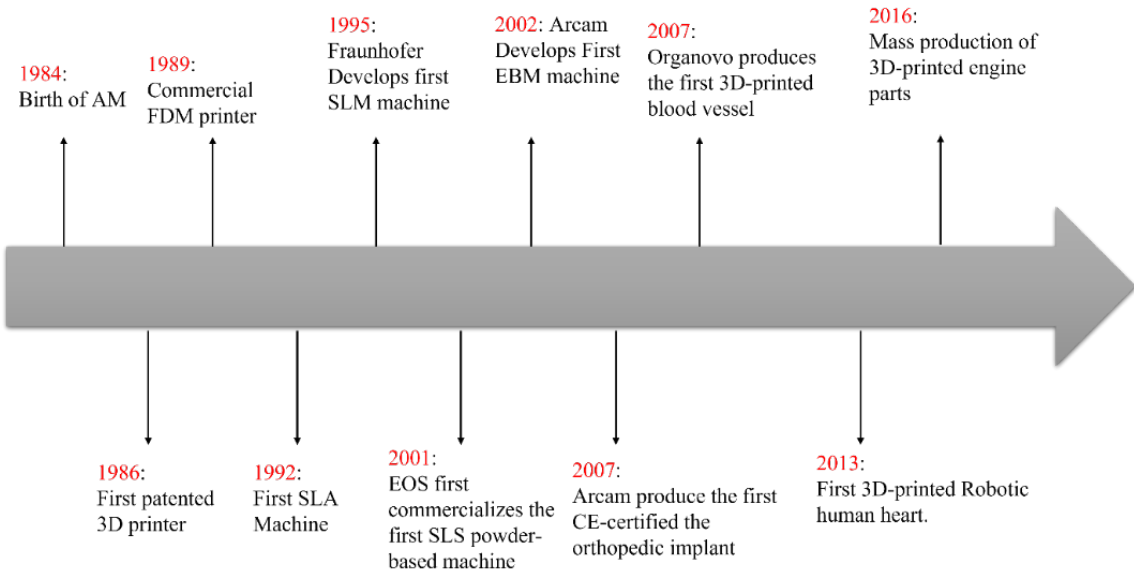

Figure 3 Chronological Representation of AM Advancements

In 1984, Chuck Hull invented stereolithography (SLA), the first commercial AM process. In 1987, Scott Crump developed Fused Deposition Modeling, a widely used AM technology. In the 1990s, selective laser sintering (SLS) and laminated object manufacturing (LOM) were invented, offering new possibilities in AM technology. The first commercial AM systems were also introduced in this decade, expanding the technology's reach. In the 2000s, advancements in AM technologies were made through improved software, materials, and equipment. Direct metal laser sintering (DMLS) and electron beam melting (EBM) were invented, expanding the range of materials available for AM. In recent years, AM technology has significantly improved speed, accuracy, and affordability. In 2010, HP developed Multi Jet Fusion, which enables the production of functional parts at a fraction of the cost and time of traditional manufacturing methods. Carbon 3D company also introduced Digital Light Synthesis (DLS) in 2015, which uses light and oxygen to produce parts with mechanical properties like injection-molded plastics. As technology improves widely, we are using desktop printers for convenience [11]. Today, AM continues to evolve, with advancements in materials, software, and hardware driving its growth. Technology has the potential to revolutionize manufacturing by offering unprecedented design freedom, reduced lead times, and cost savings [9, 11].

Several studies have explored the influence of various factors on the magnetic and mechanical properties of additively manufactured parts using different materials and technologies. Buchanan et al. and Ralchev et al. both investigated the impact of infill density and layer height on energy consumption, mass, magnetic flux density, and print time. They found that adjusting these parameters can lead to reduced print time, energy consumption, and material usage [12, 13].

In a similar vein, Bollig et al. examined the effect of the internal fill factor on magnetization and observed that higher fill factors result in decreased magnetization. Patton et al. explored the relationship between infill orientation, macroscopic shape, and magnetic susceptibility, discovering that infill orientation has a significant impact on etic properties [14].

Furthermore, Watson et al. and Henderson et al. studied the influence of print parameters and deposition direction on the magnetic properties of printed parts. Watson et al. observed that changing print parameters affected the magnetic field response, indicating the importance of filament orientation and processing conditions. Henderson et al. found that printing in the presence of a magnetic field enhanced the magnetic properties of the samples compared to those printed without a magnetic field [15, 16].

Guan et al. investigated composites filled with carbonyl iron particles, demonstrating that saturation magnetization does not have a linear relationship with filler content. They also observed improved mechanical strength in the composites compared to traditional methods [17].

Mohan et al. focused on the mechanical properties of MEX-printed parts and found that infill pattern and build orientation significantly affect mechanical performance, with denser infill patterns and vertical orientations resulting in superior mechanical properties [9].

Laureto et al. investigated copper fill, bronze fill, magnetic iron PLA, and stainless-steel PLA composites, reporting significant improvements in thermal conductivity compared to traditional materials. Oksiuta et al. studied PLA composites modified with Mg, Fe, and Polyethylene, observing increased hardness and tensile strength in iron-based specimens. Oyelaja et al. focused on PLA composites with carbon and iron particles, enhancing electrical conductivity and magnetic properties, while developing a neural network model for accurate prediction of composite properties [18–20].

Yongquan et al. explored carbonyl iron powders, finding increased density, hardness, and bending strength with higher sintering temperature and pressure. Dayue Jiang et al. investigated PLA/iron composite scaffolds for bone tissue engineering, demonstrating improved mechanical properties and degradation resistance. Huseynov et al. analyzed the thermal properties of short carbon fiber-reinforced polymer composites, emphasizing the influence of matrix materials on thermal conductivity and coefficient of thermal expansion [21, 22].

Thompson et al. and Ersoy et al. conducted studies on the printed and sintered samples using low-cost fused filament fabrication with metal composites. Thompson et al. examined the influence of printing parameters on the flexural strength of 316L steel samples and found comparable results to conventionally manufactured samples. Ersoy et al. focused on variations in the sintering process, investigating different temperatures and dwell times, and concluded that higher sintering temperatures and shorter dwell times led to better outcomes [23, 24].

Zhang et al. explored the fabrication of electrical motor parts using fused filament fabrication with an 80% iron ore composite. They assessed the processability and thermal properties of the filaments and established a two-step binding and sintering process, which resulted in a minimal loss of polymer decomposition and shrinkage [8].

According to the reviewed literature, the thermophysical and geometric properties of 3D Printed PLA parts with a high level of iron concentration have not received extensive research attention, and the influence of post-processing on their properties remains largely unexplored.

The work presented here seeks to understand how different combinations of process parameters affect these properties, providing insights into optimizing the LCMMEX process for enhanced performance and quality. This unique study will contribute to the AM body of knowledge by adding new findings to produce low-cost iron parts in a few different ways [14]. Additionally, this study aims to analyze the physical characterization of an Iron-PLA composite material[24].

Materials and Methodology

In pursuit of our research goal, this research is designed as a structured experiment with twelve distinct parameters, as outlined in Table 1. For specimen printing, this research has maintained precise conditions: nozzle temperature at 225°C, bed temperature at 65°C, and a nozzle diameter of 0.8mm. The specimens are consistently sized at 50mm x 25mm x 3mm. The material used for printing is a High percentage of Iron-PLA. Which is commercially available on the market from a virtual foundry website [25]. The parameters that have been varied include the infill percentage, layer height, and print speed. All the samples have been printed under atmospheric room temperature conditions.

The MEX process involves several steps, including the preparation of the 3D Computer-Aided Design (CAD) model, slicing of the model into individual layers, and converting the data into G-code, which controls the movement of the extruder a schematic diagram of generating G-code is shown in Figure 4. The extruder heats and melts the thermoplastic material, which is then deposited onto the building platform. Once a layer is completed, the build platform is lowered, and the process is repeated until the desired object is produced.

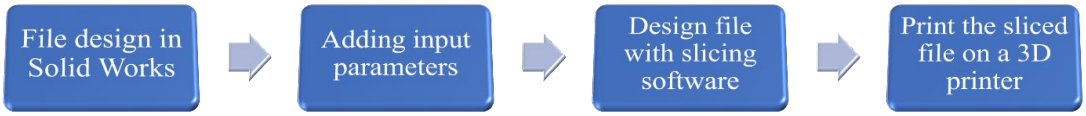

Figure 4 Steps of the Printing Process

Table 1 DOE Table

Infill Density (%)	Layer Height (mm)	Print Speed (mm/s)
100	0.1	45
100	0.2	45
100	0.1	60
100	0.2	60
60	0.1	45
60	0.2	45
60	0.1	60

60	0.2	60
20	0.1	45
20	0.2	45
20	0.1	60
20	0.2	60

Various equipment's were used to record the output variables and their respective responses in the study. The printing time variable was documented in hours, representing the duration of the printing process from the initial layer to the completion of the fabricated part. To ensure accuracy and avoid any influence from the initial print temperature, the print time was measured from the point when material extrusion commenced. This timing adjustment was necessary because it takes less time for a printer to heat a hot nozzle from 200°C to 220°C compared to heating a nozzle from 20°C to 220°C [26, 27].

The mass of each print was individually measured using a Mettler Toledo PL602 S precision balance. Before each measurement, the scale was zeroed (tared) to eliminate any measurement errors. Dimensional measurements, including length, width, and height, were collected using Ingress protection (IP)54 digital calipers on the printed parts. Height measurements were taken along the z-axis of the print direction, width measurements along the x-axis, and length measurements along the y-axis. These measurements were then compared to the designed dimensional parameters to determine the percentage difference between the measured values and the process parameters [8]

Surface roughness, which indicates changes in the surface texture, was measured in micrometers using the Mitutoyo SJ-210 Surface Roughness Equipment. Specifically, the Ra surface roughness was measured, which represents the average deviation of a measured surface. The samples were measured by keeping the part stationary while the sensor traced over the surface which are in 45° orientation. Measurements were taken on the top of the print relative to the print bed, as well as the width and length of the print [7, 28, 29].

Magnetic flux density, which characterizes the change in the total magnetic field passing through a specific surface area, was measured using the FW Bell Model 640 Gaussmeter. This device measured the magnetic flux density of the samples. A sample was placed perpendicularly between the magnet and the three-axis probe, and the resulting change in the magnetic field was measured to determine the magnetic flux density which are in different orientations. The three-axis probe was set to x, y, and z-direction, aligning with the length of the probe. The probe holder ensured the probe remained stationary, while the magnet and test sample were kept at a consistent distance of 7.5 mm from each other [9, 12, 16, 17, 30].

Thermal conductivity is a material property that measures its ability to conduct heat. It describes how quickly heat can flow through a material when there is a temperature difference. It is typically measured in watts per meter-kelvin (W/mK). High thermal conductivity allows for fast heat transfer, while low thermal conductivity indicates poor heat conduction. In AM, thermal conductivity is crucial for managing heat during the printing process, selecting

appropriate materials, optimizing energy consumption, and ensuring the performance and functionality of printed parts. The heat transfer rate in one-dimensional conduction through a cylindrical cross-section is given by Fourier's law, where the thermal conductivity and temperature gradient play key roles. Experimental setups involve thermocouples, brass cylinders, and water cooling to measure thermal conductivity accurately [18, 19, 27, 31].

To conduct the ANOVA analysis, the relevant R code was written and uploaded into the software. The code included specifications for the response variable and input variables of interest. As part of the analysis, any outliers present in the dataset were identified and subsequently removed from the analysis data. This step was taken to ensure the robustness and accuracy of the results obtained from the ANOVA analysis.

Steps for analysis of ANOVA in R software:

1. Install and Load Required Packages: Begin by installing and loading the necessary R packages for ANOVA analysis, such as stats and car. Use the install Packages () and library () functions to install and load the packages, respectively.
2. Import and Prepare Data: Import the dataset containing the relevant variables for analysis, including the response variable (e.g., surface roughness, weight, dimensional accuracy) and the factors of interest (e.g., infill density, layer height). Ensure that the data is properly formatted and stored in a suitable structure, such as a data frame.
3. Check Assumptions: Assess the assumptions of ANOVA, such as normality and equal variance. Use diagnostic plots, such as residual plots (plot () function) or normality plots (qqPlot () function from the car package), to evaluate these assumptions. If the assumptions are violated, consider transformations or alternative non-parametric tests.
4. Perform ANOVA Analysis: Use the aov () function in R to conduct the ANOVA analysis. Specify the formula using the ~ symbol, with the response variable followed by the factors of interest. For example, aov_model <- aov(response variable ~ factor1 + factor2, data = your_data).
5. Check ANOVA Results: Utilize the summary () function to examine the ANOVA results. This will provide an overview of the analysis, including the F-statistic, p-value, and degrees of freedom for each factor. Assess the significance of each factor's effect on the response variable based on the p-values.
6. Perform Posthoc Tests: If the ANOVA results indicate significant differences between factor levels, conduct posthoc tests to determine specific pairwise differences. Commonly used posthoc tests in R include the TukeyHSD () function from the stats package or the glht () function from the multicopy package. These tests allow for pairwise comparisons and provide adjusted p-values.

Results and Discussion

The subsequent sections will focus on the analysis of process-related parameters to provide practical insights for practitioners in the field of AM. These findings aim to assist AM professionals by offering valuable guidance based on statistical analysis and data-driven results. The analysis was performed using the ANOVA method with the aid of R software. By following this approach, the analysis aimed to uncover significant relationships and variations among the process-related parameters in AM. The findings obtained from the ANOVA analysis, conducted using R software, will contribute to the understanding and improvement of AM

processes, enabling practitioners to make informed decisions based on the statistical evidence derived from the data.

Analysis of Magnetic Susceptibility

Table 2 reveals the significant impact on magnetic susceptibility due to all examined input variables. Infill density demonstrates the greatest influence, with 81.3% of the observed variation as shown in Figure 5. Figure 6 and Figure 7 display the layer height and print speed contribution, which is less than 5% each to the overall variation. Higher infill density leads to increased magnetic susceptibility due to a greater amount of iron material in the print. The samples exhibit magnetic properties sufficient to attract magnetized objects, with the highest susceptibility of 0.7 Gauss found in 100% infill density samples and the lowest of 0.21 Gauss in 20% infill density samples.

Table 2 ANOVA Measurements for Magnetic Susceptibility Measurements

	Sum of square	DF	F value	Pr (>F)	Mean Square
Infill density	0.192626	1	38.7638	0.000154	0.192626
Layer height	0.000376	1	0.0756	0.7921434	0.000376
Print speed	0.004241	1	0.8381	0.3866950	0.004241

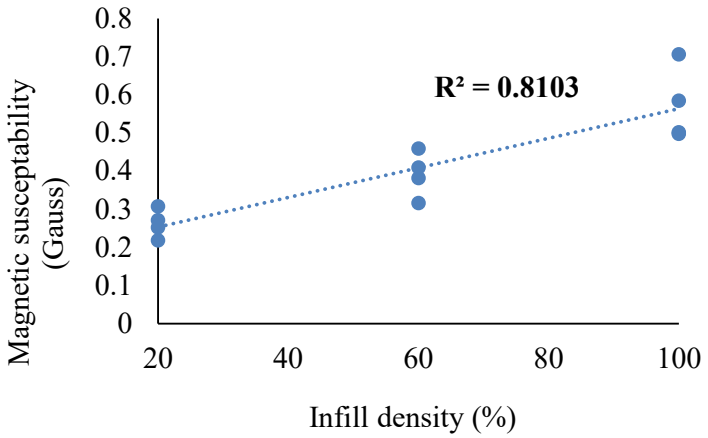

Figure 5 Infill Density vs Magnetic Susceptibility Plot

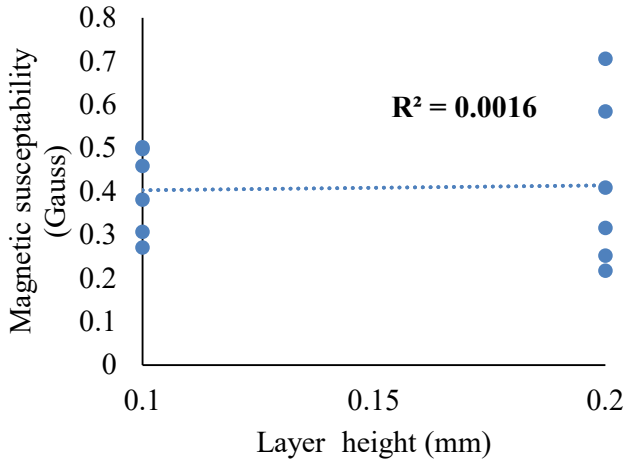

Figure 6 Layer Height vs Magnetic Susceptibility Plot

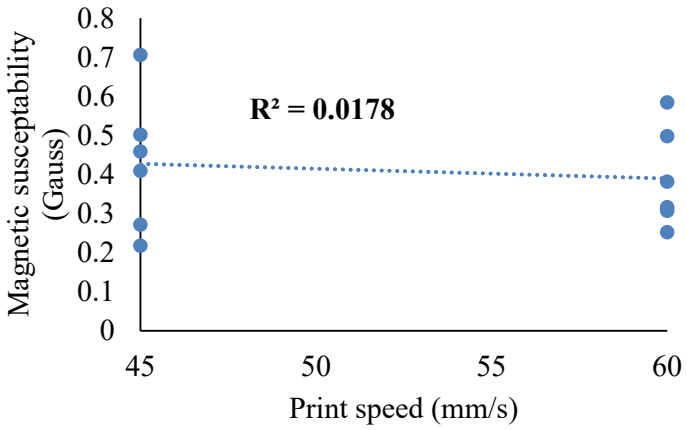

Figure 7 Print Speed vs Magnetic Susceptibility Plot

Analysis of Thermal Conductivity

The analysis using R software which was shown in Table 3 indicates that high iron content samples in AM have significantly higher thermal conductivity compared to PLA samples. The most influential factor determining thermal conductivity is infill density. High iron samples exhibit a thermal conductivity of 10.5 W/mK, with a low mean square error for infill density is 12.48 and a p-value of 0.0001882, indicating a highly significant difference. The data variability is illustrated in Figure 9 and Figure 10. Although print speed and layer height also contribute, infill density has a greater impact on thermal conductivity which was shown in Figure 8 it has an R-squared value of 0.834. These findings highlight the importance of material composition in heat transfer properties and suggest the potential use of high iron content materials for applications requiring enhanced thermal conductivity in AM parts.

Table 3 ANOVA Results for Thermal Conductivity Measurements

	DF	Sum of Square	Mean square	F value	P(>F)
Infill density	1	12.4800	12.4800	42.2413	0.0001882
Layer height	1	0.0203	0.0203	0.0688	0.7996734
Print speed	1	0.0994	0.0994	0.3363	0.5779099

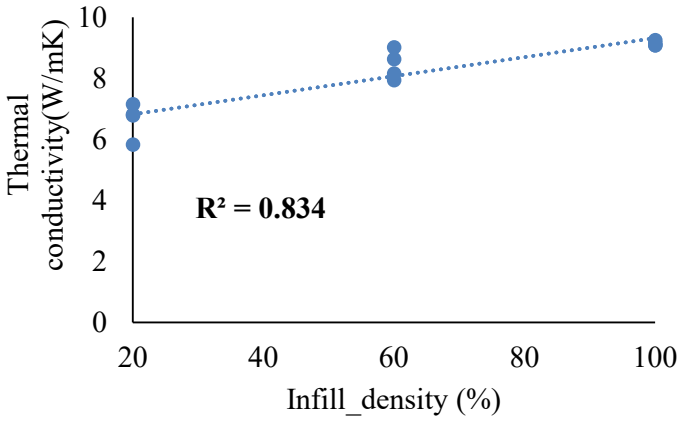

Figure 8 Infill Density vs Thermal Conductivity

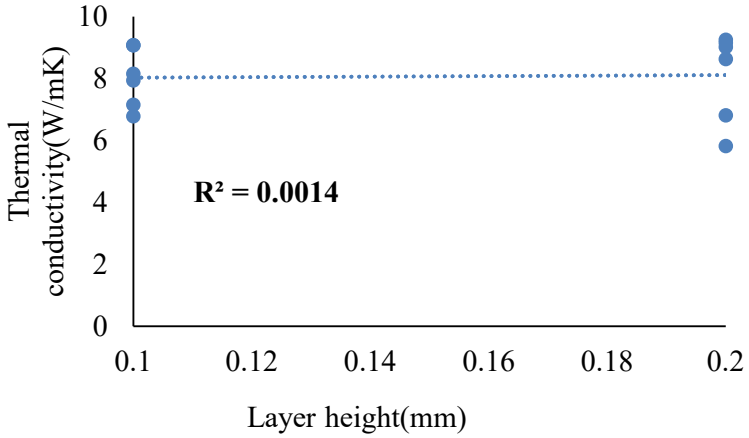

Figure 9 Thermal Conductivity vs Layer Height Plot

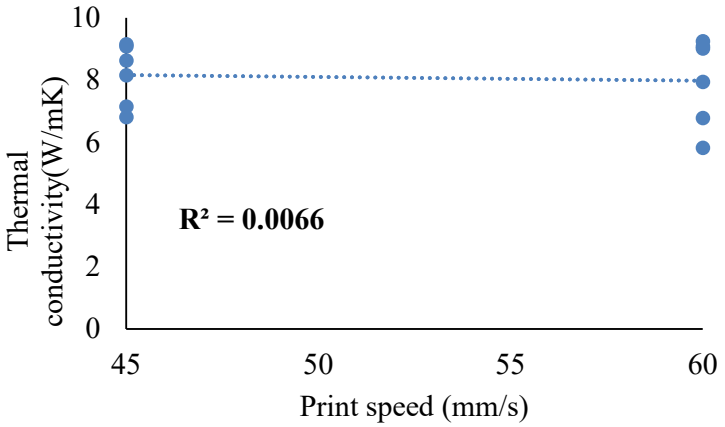

Figure 10 Thermal Conductivity vs Print Speed Plot

Analysis of Mass Data

Table 4 presents findings of mass measurements. However, print speed and layer height do not demonstrate a significant effect in this regard. Specifically, a higher infill density is associated with an increase in mass, and infill density alone accounts for 75.35% of the observed variability, as shown in Figure 11.

On the other hand, the influence of layer height and print speed on mass is found to be negligible, explaining less than 1% of the variability, as illustrated in Figure 12. Interestingly, increasing layer height tends to decrease the variability in mass, which could be attributed to factors such as accidental over-extrusion or reduced voids between layers. Conversely, the effect of print speed on mass, as depicted in Figure 13, is relatively insignificant.

Table 4 ANOVA Results for Mass Measurements

	Sum of Square	DF	F value	P(>F)
Infill density	4.8655	1	27.6068	0.0005247
Layer height	0.0052	1	0.0293	0.8378969
Print speed	0.0245	1	0.014	0.745453

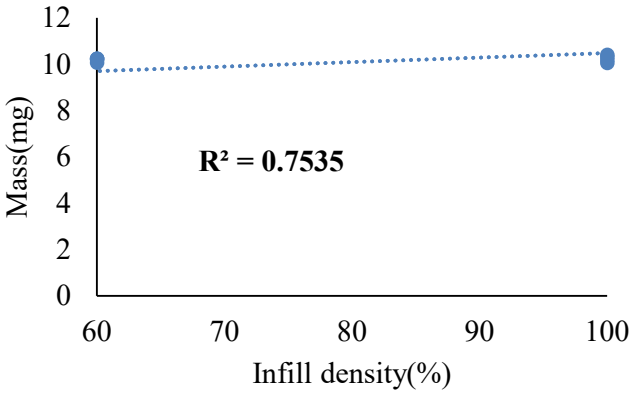

Figure 11 Infill Density vs Mass Plot

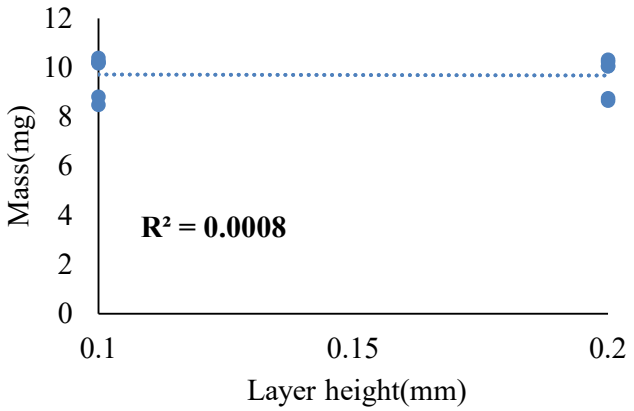

Figure 12 Layer Height vs Mass Plot

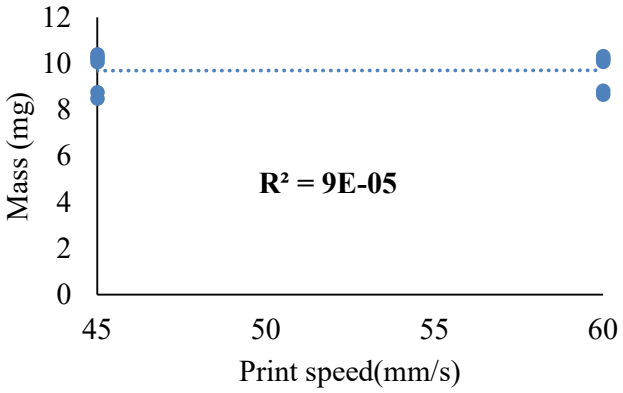

Figure 13 Print Speed vs Mass Plot

Analysis of Print Time Data

The interpretation of the ANOVA results shown in Table 5 reveals valuable insights into the relationship between the response variable, print time, and the three examined factors: infill

density, layer height, and print speed. The analysis indicates that layer height exhibits a significant impact on print time, as evidenced by its substantial sum of squares, high F value (689.7959), and exceptionally low p-value (4.746e-09). These findings suggest that variations in layer height significantly affect the time required for printing. On the other hand, infill density demonstrates a smaller sum of squares and a p-value (0.08311) above the conventional significance level of 0.05, implying that its influence on print time may not be statistically significant. Similarly, print speed exhibits a relatively low F value (1.7839) and a p-value (0.218415) above the threshold, indicating that it may not have a substantial effect on print time. These interpretations highlight the importance of considering layer height as a critical determinant of print time while suggesting that infill density and print speed may have a negligible impact in this specific context. The ANOVA results are also in accordance with the statistical R^2 values calculated in Figure 14-Figure 16.

Table 5 ANOVA Results for Print Time Data

	Sum of square	DF	F value	P(>F)
Infill density	2	1	3.9184	0.08311
Layer height	352.08	1	689.7959	4.746e-09
Print speed	18.750	1	1.7839	0.218415

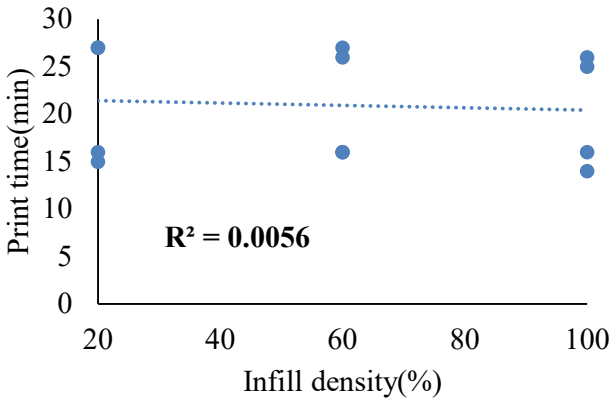

Figure 14 Infill Density vs Print Time Plot

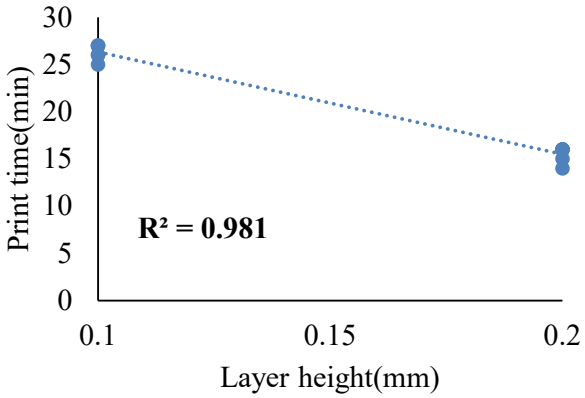

Figure 15 Layer Height vs Print Time Plot

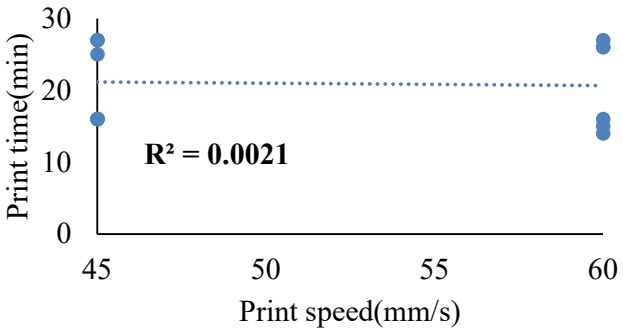

Figure 16 Print Speed vs Print Time Plot

Analysis of Dimensional Variation Data

Analysis of Length Variation Data

The findings presented in Table 6 demonstrate that none of the p-values associated with the input variables achieve statistical significance at the 0.05 threshold. Consequently, it can be concluded that the input variables do not exert a significant influence on the dimensional variation of length. This conclusion is further supported by the regression analysis depicted in Figure 17-Figure *19*, which consistently indicate a lack of significance. These results suggest that factors other than the selected input variables play a more critical role in determining the dimensional variation along the length or X-axis. Consequently, it can be inferred that the chosen input variables do not have a noticeable impact on the dimensions when compared to the original dimensions. The analysis underscores the higher accuracy offered by the Prusa technology in this regard.

The collected data yields an average deviation of approximately 0.5% below the originally intended length, implying that the length tends to be slightly shorter than the design specification.

Table 6 ANOVA Analysis of Dimensional Accuracy in X Direction

	Estimate	Standard error	T value	P (>l t l)
Infill density	0.0012361	0.0003564	3.469	0.846471
Layer height	-0.0537037	0.2327677	-0.231	0.82332
Print speed	-0.0005062	0.0015518	-0.326	0.075265

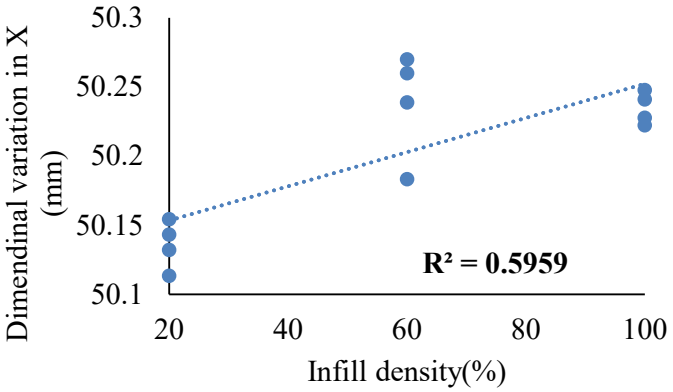

Figure 17 Infill Density vs Dimensional Variation in X Direction Plot

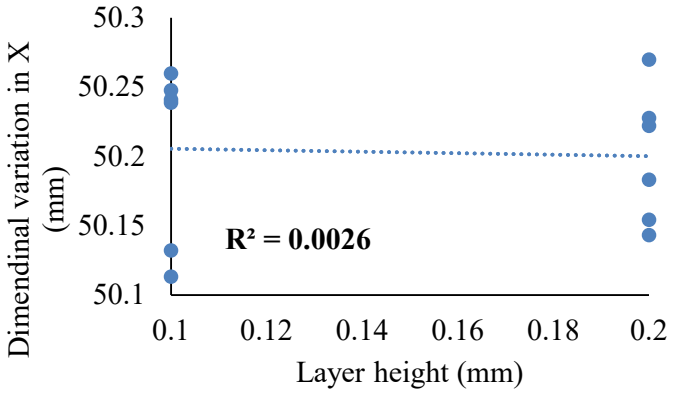

Figure 18 Layer Height vs Dimensional Variation in X Direction Plot

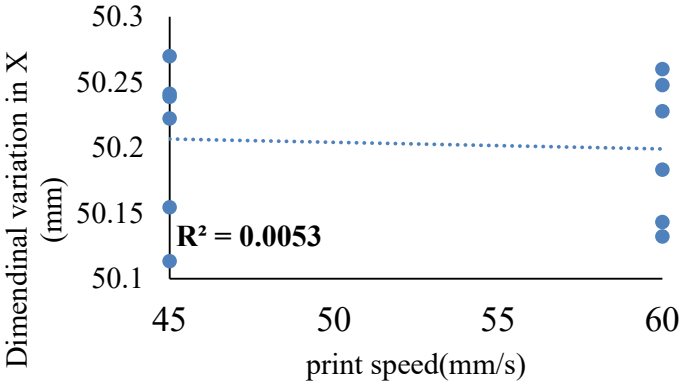

Figure 19 Print Speed vs Dimensional Variation in X Direction Plot

Analysis of Width Variation Data

According to the results presented in Table 7, none of the p-values associated with the input variables reaches the critical threshold of 0.05. This indicates that none of the input variables has a significant impact on the dimensional variation of width. This lack of significance is further supported by the regression analysis depicted in Figure 21-Figure *22*, which demonstrate a consistent pattern of insignificance. It becomes evident that variables

other than the selected input variables play a more significant role in determining the dimensional variation along the x-axis.

The collected data indicates that, on average, the width deviates by approximately 0.5% from the originally intended width. This implies that the actual width tends to be slightly smaller than the designed width.

Table 7 ANOVA Analysis of Dimensional Accuracy in the Y Direction

	Estimate	Standard error	T value	P (>l t l)
Infill density	-0.0004097	0.606508	412.482	0.1196
Layer height	0.3222222	0.1535893	2.098	0.2692
Print speed	0.0013827	0.0010239	1.350	0.2138

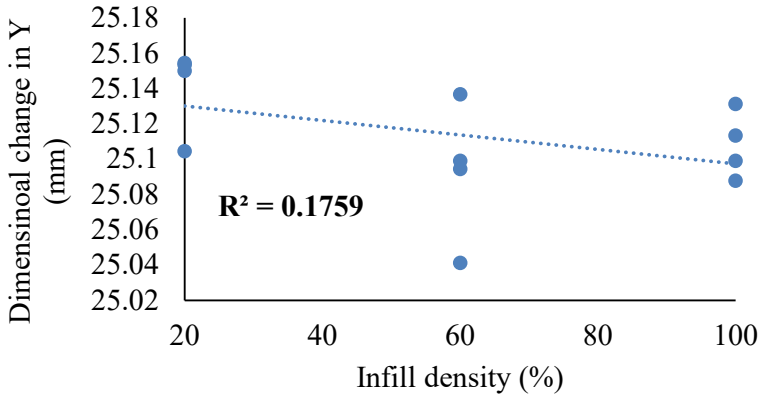

Figure 20 Infill Density vs Dimensional Change in Y Direction Plot

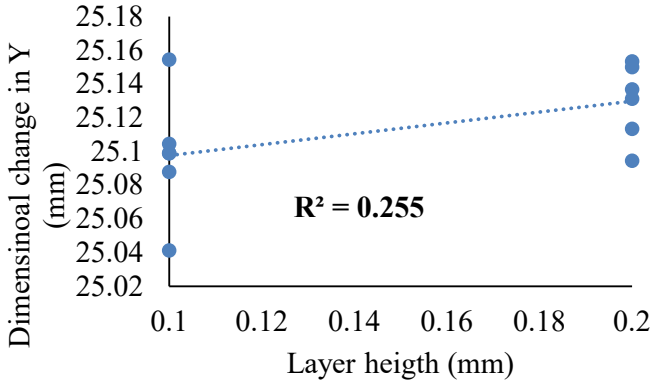

Figure 21 Layer Height vs Dimensional Change in Y Direction Plot

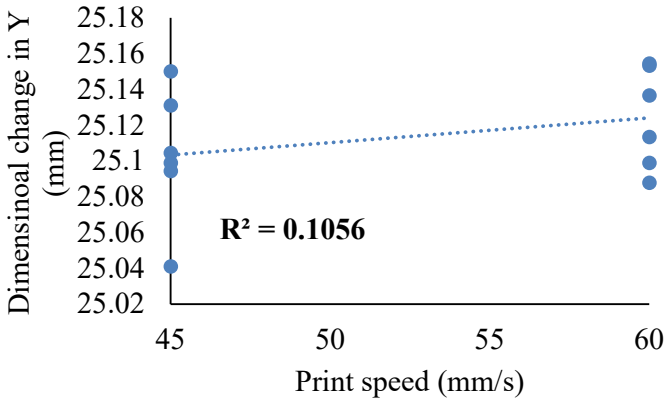

Figure 22 Print Speed vs Dimensional Change in Y Direction Plot

Analysis of Height Variation Data

Table 8 provides substantial evidence that none of the input variables significantly contribute to the dimensional variation in material height. This finding is further supported by the regression analyses presented in Figure 23-Figure 25, which align with the results of the ANOVA tests.

It is worth noting that the average height deviates by approximately 8.05% from the originally designed height. This notable discrepancy indicates an overestimation in height compared to the slight underestimations observed in the width and length dimensions. The consistent overestimation in height is a significant observation, as it stands in contrast to the intended parameters established during the design phase.

Table 8 ANOVA Analysis Table for Dimensional Change in Z Direction

	Estimate	Standard error	T value	P (>l t l)
Infill density	0.0015590	0.0008556	14.068	0.106
Layer height	-0.0111111	0.5588952	-0.020	0.985
Print speed	-0.0009630	0.0037260	-0.258	0.803

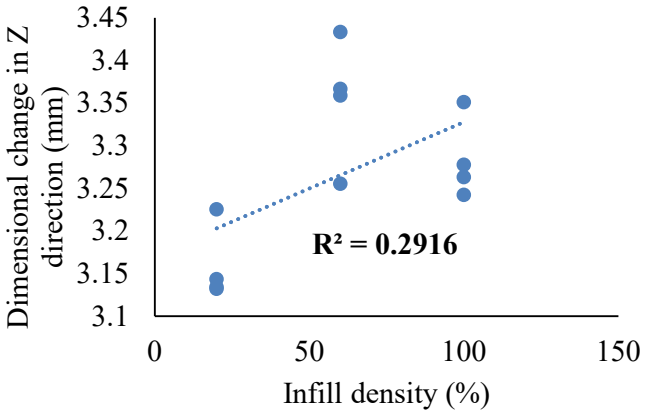

Figure 23 Infill Density vs Dimensional Change in Z Direction Plot

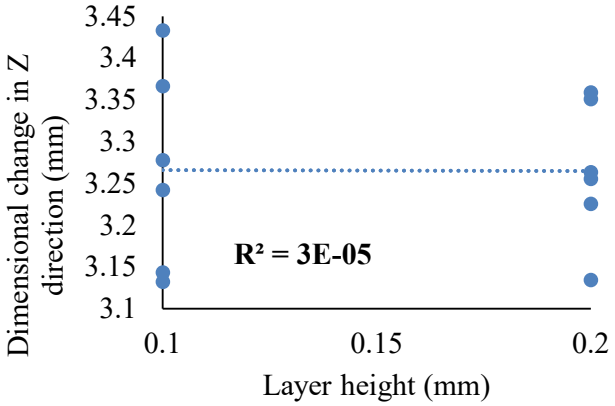

Figure 24 Layer Height vs Dimensional Change in Z Direction Plot

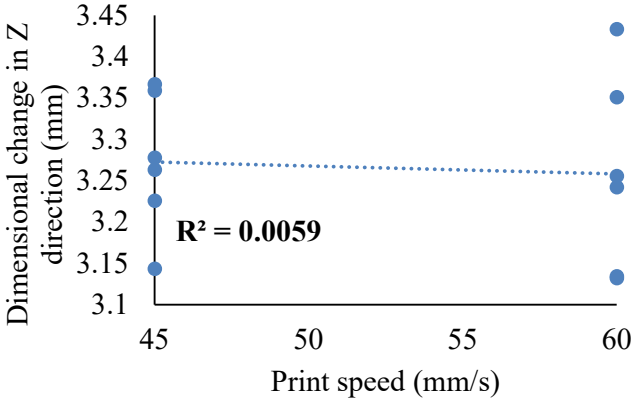

Figure 25 Print Speed vs Dimensional Change in Z Direction Plot

Analysis of Surface Roughness

Table 9 displays the examined input variables in the study, and it is evident that infill density holds the highest influence, explaining a substantial 78.06% of the observed variation, as depicted in Figure 26. The significance of infill density surpasses that of the other two input

variables significantly. This finding is logical, as an increase in infill density results in a greater mass of iron material within the 3D print, ultimately leading to elevated surface roughness.

In contrast, the analysis reveals that both layer height and print speed have minimal contributions, each explaining less than 1% of the overall variation in the data, as illustrated in Figure 27-Figure *28*, respectively. Interestingly, it is observed that neither layer height nor print speed has a significant impact on surface roughness. On the other hand, infill density emerges as the dominant and more influential factor, clearly indicating its strong association with surface roughness.

Table 9 ANOVA Analysis Table for Surface Roughness Measurement

	Estimate	Standard error	T value	P (>l t l)
Infill density	-0.018884	0.901033	-5.406	0.000641
Layer height	0.640000	2.281737	0.280	0.786220
Print speed	0.005622	0.015212	0.370	0.721272

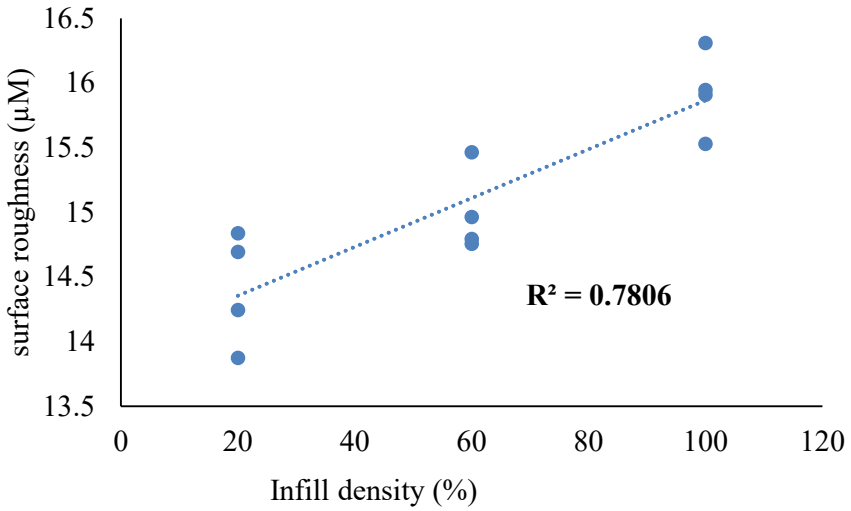

Figure 26 Surface Roughness vs Infill Density Plot

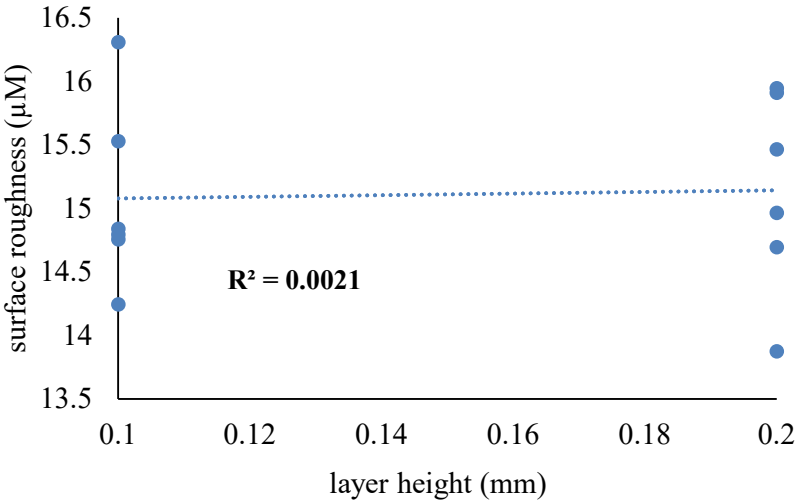

Figure 27 Layer Height vs Surface Roughness Plot

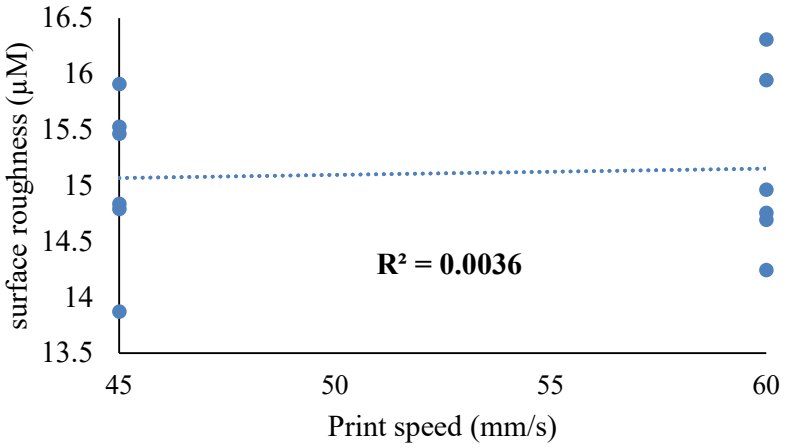

Figure 28 Print Speed vs Surface Roughness Analysis Plot

Conclusion and Future Work

The analysis conducted in this study yields significant findings regarding the impact of various input variables on output responses in LCMMEX process. Overall, it is evident that all input variables, namely infill density, layer height, and print speed, play a substantial role in influencing the output responses. Among them, infill density emerges as the most influential input variable, followed by layer height and print speed, respectively. Notably, these input variables have specific effects on different properties of the printed structures. In terms of magnetic properties, infill density significantly influences magnetic susceptibility, allowing for tailored magnetic properties in 3D-printed structures. Regarding thermal conductivity, layer height proves to be a critical factor, as smaller heights result in enhanced thermal conductivity by reducing air gaps and facilitating improved thermal transfer between layers. Surface roughness is significantly impacted by both infill density and layer height, with higher densities and smaller heights leading to smoother surfaces in AM. Furthermore, infill density primarily determines the weight of printed parts, as higher densities correspond to increased weight due to greater material volume. Lastly, layer height plays a vital role in achieving dimensional accuracy, with smaller heights contributing to improved precision and consistency in the

dimensions of 3D-printed parts. In conclusion, this study establishes the significance of all input variables in shaping the output responses across various aspects of LCMMEX process, providing valuable insights for optimizing the printing process and enhancing the quality of printed structures.

For future work, exploring higher percentages of iron and sintering processes can be investigated to achieve higher material density, enabling applications in electromagnetic devices like actuators, transformers, and sensors. Additionally, ongoing research is exploring the use of higher iron percentage composites in energy harvesting devices.

Acknowledgments

The financial and technical support provided by the Mechanical Engineering Department, Physics Department, and Manufacturing and Engineering Technology Department is greatly appreciated. Magnetic susceptibility studies have been carried out in Dr. Rajabali's lab which is supported by the DOE Office of Science through Grant No. DE-SC0016988.

References

1. Hasanov S, Gupta A, Alifui-Segbaya F, Fidan I (2021) Hierarchical homogenization and experimental evaluation of functionally graded materials manufactured by the fused filament fabrication process. Compos Struct 275:114488. https://doi.org/10.1016/J.COMPSTRUCT.2021.114488

2. ASTM Additive Manufacturing Standards | Quality | Stratasys Direct. https://www.stratasys.com/en/stratasysdirect/resources/articles/astm-additive-manufacturing-standards-what-you-need-to-know/. Accessed 20 Jun 2023

3. The 7 Types of Additive Manufacturing - Carbon. https://www.carbon3d.com/resources/blog/the-7-types-of-additive-manufacturing. Accessed 15 May 2023

4. Fidan I, Imeri A, Gupta A, et al (2019) The trends and challenges of fiber reinforced additive manufacturing. International Journal of Advanced Manufacturing Technology 102:1801–1818. https://doi.org/10.1007/S00170-018-03269-7/METRICS

5. Alshaikh Ali M, Fidan I, Allen M, et al (2022) Utilizing Lattice Infill Structures to Optimize Weight with Structural Integrity Investigation for Commonly Used 3D Printing Technologies. https://doi.org/10.26153/TSW/44430

6. Alkunte S, Fidan I, Hasanov S (2022) Experimental Analysis of Functionally Graded Materials produced by Fused Filament Fabrication. https://doi.org/10.26153/TSW/44144

7. Ali MA, Fidan I, Tantawi K (2023) Investigation of the impact of power consumption, surface roughness, and part complexity in stereolithography and fused filament fabrication. International Journal of Advanced Manufacturing Technology 126:2665–2676. https://doi.org/10.1007/S00170-023-11279-3/METRICS

8. Zhang Z, Femi-Oyetoro J, Fidan I, et al (2021) Prediction of Dimensional Changes of Low-Cost Metal Material Extrusion Fabricated Parts Using Machine Learning Techniques. Metals 2021, Vol 11, Page 690 11:690. https://doi.org/10.3390/MET11050690

9. Mohan S, Student RG (2022) Effect of infill pattern and build orientation on mechanical properties of FDM printed parts: An experimental modal analysis approach

10. Fidan I, Huseynov O, Ali MA, et al (2023) Recent Inventions in Additive Manufacturing: Holistic Review. Inventions 2023, Vol 8, Page 103 8:103. https://doi.org/10.3390/INVENTIONS8040103

11. (1) New Messages! https://markforged.com/resources/blog/additive-manufacturing-history. Accessed 20 Jun 2023

12. Ralchev M, Mateev V, Marinova I (2021) Magnetic properties of FFF/FDM 3D printed magnetic material. 2021 17th Conference on Electrical Machines, Drives and Power Systems, ELMA 2021 - Proceedings. https://doi.org/10.1109/ELMA52514.2021.9503037

13. Buchanan R, Kumar Dasari J, Fidan I, et al (2022) Knowledge Base Development for Mechanical Properties and Energy Consumption of Iron-PLA Composite Filaments in Additive Manufacturing. https://doi.org/10.26153/TSW/44539

14. Bollig LM, Patton M V., Mowry GS, Nelson-Cheeseman BB (2017) Effects of 3-D Printed Structural Characteristics on Magnetic Properties. IEEE Trans Magn 53:. https://doi.org/10.1109/TMAG.2017.2698034

15. Henderson L, Zamora S, Ahmed TN, et al (2021) Altering magnetic properties of iron filament PLA using magnetic field assisted additive manufacturing (MFAAM). J Magn Magn Mater 538:168320. https://doi.org/10.1016/J.JMMM.2021.168320

16. Watson ND, Von Lockette P (2018) Deposition Controlled Magnetic Alignment in Iron-PLA Composites. https://doi.org/10.26153/TSW/17113

17. Guan XN, Xu XN, Kuniyoshi R, et al (2018) Electromagnetic and mechanical properties of carbonyl iron powders-PLA composites fabricated by fused deposition modeling. Mater Res Express 5:115303. https://doi.org/10.1088/2053-1591/AADCE4

18. Laureto J, Tomasi J, King JA, Pearce JM (2017) Thermal properties of 3-D printed polylactic acid-metal composites. Progress in Additive Manufacturing 2:57–71. https://doi.org/10.1007/S40964-017-0019-X/FIGURES/15

19. Oksiuta Z, Jalbrzykowski M, Mystkowska J, et al (2020) Mechanical and Thermal Properties of Polylactide (PLA) Composites Modified with Mg, Fe, and Polyethylene (PE) Additives. Polymers 2020, Vol 12, Page 2939 12:2939. https://doi.org/10.3390/POLYM12122939

20. Oyelaja HB, Wu N, Ojo OA (2020) Fabrication and characterization of plastics with electrical and magnetic properties. International Journal of Advanced Manufacturing Technology 106:3451–3462. https://doi.org/10.1007/S00170-019-04853-1/METRICS

21. Jiang D, Ning F, Wang Y (2021) Additive manufacturing of biodegradable iron-based particle reinforced polylactic acid composite scaffolds for tissue engineering. J Mater Process Technol 289:116952. https://doi.org/10.1016/J.JMATPROTEC.2020.116952

22. Ye Y, Li X, Cheng Z, et al (2017) The influence of sintering temperature and pressure on microstructure and mechanical properties of carbonyl iron powder materials fabricated by electric current activated sintering. Vacuum 137:137–147. https://doi.org/10.1016/J.VACUUM.2016.12.044

23. Thompson Y, Gonzalez-Gutierrez J, Kukla C, Felfer P (2019) Fused filament fabrication, debinding and sintering as a low cost additive manufacturing method of 316L stainless steel. Addit Manuf 30:100861. https://doi.org/10.1016/J.ADDMA.2019.100861

24. Murat Ersoy N, Murat Aydoğdu H, Ünalan Değirmenci B, et al (2015) The effects of sintering temperature and duration on the flexural strength and grain size of zirconia. https://mc.manuscriptcentral.com/iabo 1:43–50. https://doi.org/10.3109/23337931.2015.1068126

25. High Carbon Iron Filamet™ | 3D Printing | FFF/FDM printers | Metal 3D Print - The Virtual Foundry. https://shop.thevirtualfoundry.com/collections/filamet/products/high-carbon-iron-filamet?variant=29486020165715. Accessed 2 May 2023

26. Norris M, Fidan I, Allen M (2022) Rheological Characterization of Room Temperature Powder Metal Paste for Extruded Material Modeling. https://doi.org/10.26153/TSW/44186

27. Gupta A, Hasanov S, Fidan I (2022) Thermal characterization of short carbon fiber reinforced high temperature polymer material produced using the fused filament fabrication process. J Manuf Process 80:515–528. https://doi.org/10.1016/J.JMAPRO.2022.06.024

28. Zhang Z, Fidan I (2022) Machine Learning-Based Void Percentage Analysis of Components Fabricated with the Low-Cost Metal Material Extrusion Process. Materials 2022, Vol 15, Page 4292 15:4292. https://doi.org/10.3390/MA15124292

29. Surftest SJ-210 Mitutoyo Series 178 Portable Surface Roughness Tester. https://store.gaging.com/surftest-sj-210-mitutoyo-series-178-portable-surface-roughness-testers?msclkid=91f29a12ff2f1f692872fe407c74e6c2. Accessed 2 May 2023

30. F.W. Bell 640 Incremental Gaussmeter - Price, Specs. https://www.artisantg.com/Scientific/50975-1/F-W-Bell-640-Incremental-Gaussmeter. Accessed 2 May 2023

31. Heat Transfer | PA Hilton. https://www.p-a-hilton.co.uk/products/heat-transfer. Accessed 2 May 2023